to this singularity manifold is then given when the diagonal elements $a_{kk}'=0$ and the $\frac{1}{2}(m-1)(m-2)$-mass envelope is taken over the remaining nondiagonal elements $\tilde{a}_{kl}'>0$.[10]

The connection with the Landau singularity manifold with physical internal masses lies then in redefining a distorted $\Xi_n(t)$ manifold, called the $\Xi_n'(t)$ manifold, which is now parameterized by t, $(n-1)$ diagonal $a_{kk}\geqslant 0$, and $\frac{1}{2}(n-1)(n-2)$ nondiagonal $a_{kl}\leqslant 0$. For $n=4$, the $\frac{1}{2}(n-1)(n-2)$-mass envelope of this $\Xi_4'(t)$ manifold gives the (DANAD)′ manifold discussed in paper I. Note that the right-hand side of (16) has a one-parameter integral representation[8] with the explicit denominator $[\Xi_4(t)]^{1/2}$. It is therefore possible to continue analytically both sides to the physical masses.

To what extent it is possible to recover the analyticity properties of the Feynman amplitude $H_n(z;m^2)$ itself from those of the Hankel transform I_n remains to be discussed. As far as the analyticity properties in the external momentum variables z_{kl} of the p-space perturbation functions are concerned, we could very well consider functions which are superpositions of graphs $\mathcal{G}_n$ (for a given n) with arbitrary internal masses, i.e., integral of H_n over internal masses with arbitrary weight functions. The *maximal* singularity manifolds in z that are, in principle, allowed for the p-space perturbation functions with such superpositions will then be the Landau singularity manifolds $\mathfrak{L}_n(z;\hat{a})$ discussed in I, when considered over the totality of the Riemann surfaces.[11]

[10] G. Källén, Nuclear Phys. **25**, 568 (1960).

ACKNOWLEDGMENT

The author is greatly indebted to Professor G. Källén for his interest and encouragement.

[11] A similar situation holds in x space: The maximal singularity manifolds for the vacuum expectation values is given by those from the Δ_n^+ functions.

PHYSICAL REVIEW VOLUME 135, NUMBER 1B 13 JULY 1964

π^--p Interactions at 604 MeV*†

C. N. VITTITOE,‡ B. R. RILEY, W. J. FICKINGER,§ V. P. KENNEY,‖ J. G. MOWAT, AND W. D. SHEPHARD‖
University of Kentucky, Lexington, Kentucky

(Received 2 August 1963; revised manuscript received 5 March 1964)

The interactions of 604 MeV π^- mesons in a hydrogen bubble chamber have been systematically analyzed. In 33 000 pictures a total of 8052 usable events were found, corresponding to cross sections of 18.9±1.3 mb for σ(elastic), 4.98±0.54 mb for $\sigma(\pi^-p\pi^0)$, 7.87±0.91 mb for $\sigma(\pi^-n\pi^+)$, 14.0±1.0 mb for σ(neutrals), with σ(two-pion production) <0.2 mb, for a total cross section of 45.9±1.9 mb at this energy. The angular distribution for elastic scattering was fitted with a fifth-order polynomial in cosθ which gave a value of $d\sigma/d\Omega(0°)$ consistent with dispersion theory. The pion-pion effective-mass distributions for both single-pion-production channels showed pronounced peaking at high mass values, strongly inconsistent with simple isobar-production kinematics. Simple one-pion exchange does not appear to play a significant role.

I. INTRODUCTION

PION production above the ρ threshold is known to be dominated by reactions in which the pion resonance states are excited.[1–5] At lower energies it might be expected that most of the interaction would proceed through isobar-production channels,[6] with some possible $T=0$ effect due to the ABC phenomenon.[7] This paper reports evidence of peaking in the effective-mass distributions of both pion-production channels which is inconsistent with the conventional isobar picture, and which suggests that the reaction mechanism is considerably more complicated than has heretofore been expected.[8]

* Supported in part by the National Science Foundation.

† A portion of this work has been submitted by C. N. Vittitoe in partial fulfillment of the requirements for the degree of Doctor of Philosophy at the University of Kentucky.

‡ Supported in part by Southern Fellowships Fund and Kentucky Research Foundation fellowships. Present address: Ohio University, Athens, Ohio.

§ Present address: Centre d'Études Nucléaires de Saclay, France.

‖ Present address: University of Notre Dame, Notre Dame, Indiana.

[1] A. R. Erwin, R. March, W. D. Walker, and E. West, Phys. Rev. Letters **6**, 628 (1961).

[2] D. Stonehill, C. Baltay, H. Courant, W. Fickinger, E. C. Fowler *et al.*, Phys. Rev. Letters **6**, 624 (1961); D. L. Stonehill and H. Kraybill, Rev. Mod. Phys. **34**, 503 (1962).

[3] J. A. Anderson, V. X. Bang, P. G. Burke, D. D. Carmony, and N. Schmitz, Phys. Rev. Letters **6**, 365 (1961).

[4] A. Pevsner, R. Kraemer, M. Nussbaum, C. Richardson, P. Schlein *et al.*, Phys. Rev. Letters **7**, 421 (1961).

[5] V. P. Kenney, W. D. Shephard, and C. D. Gall, Phys. Rev. **126**, 736 (1962).

[6] R. M. Sternheimer and S. J. Lindenbaum, Phys. Rev. **123**, 333 (1961).

[7] N. E. Booth, A. Abashian, and K. M. Crowe, Phys. Rev. Letters **7**, 35 (1961).

[8] See, for example, the rapporteur talk of G. Puppi, *Proceedings of the 1962 International Conference on High Energy Physics at* CERN (CERN Scientific Information Service, Geneva, 1962), p. 722.

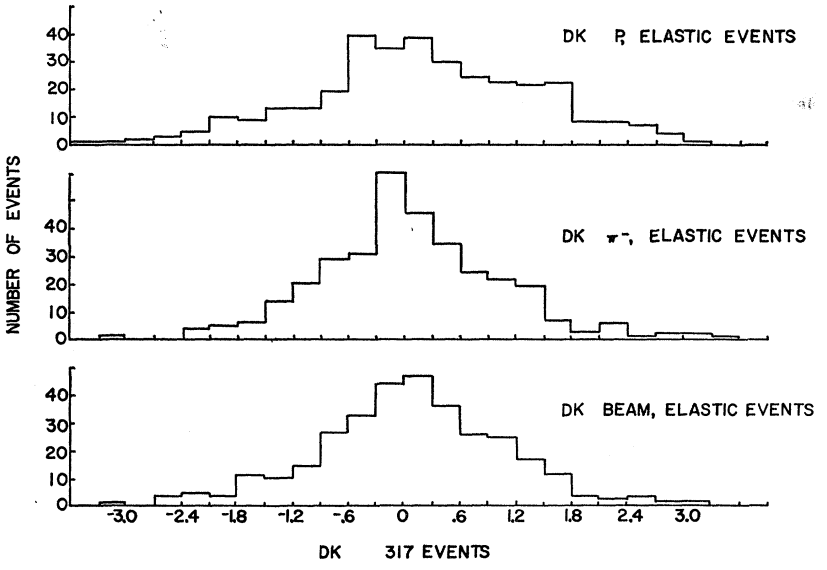

FIG. 1. Distributions of DK, the fractional adjustment of the measured curvatures, for 317 elastic events.

The π^-,p reaction has been studied with good statistics in a hydrogen bubble-chamber experiment at 604 MeV. Similar experiments carried out by a Carnegie Tech-Maryland collaboration in the same beam at 558 and 650 MeV are reported elsewhere.[9] Elastic events have been fitted to a cosine power polynomial, consistent with dispersion theory, and pion production is discussed in terms of the isobar formalism, the one-pion exchange model,[10] and other pertinent theory.

II. EXPERIMENTAL PROCEDURE

The Adair 14-in. bubble chamber was filled with hydrogen at a neon vapor pressure of 51±1 cm Hg corresponding to a hydrogen density of 0.0626±0.0001 g/cc.[11] The chamber was operated in a magnetic field given by

$$B(\text{kG}) = 17.045 + 0.00747z^2 - 0.00511r^2 + 0.0000105z^2r^2,$$

where r is the radial distance, in cm, from the chamber central axis and z is the displacement, in cm, from the chamber central plane.[12] The pictures were taken by 3 cameras mounted approximately at the corners of an equilateral triangle with 37.0 cm sides, 92.6 cm from, and parallel to, the front glass of the bubble chamber. Two fiducial marks, 25 cm apart, on the inside of the front window provide the reference marks for measurements on the pictures.

A negative pion beam of momentum 731±23 MeV/c was directed into the bubble chamber. The average momentum and momentum spread of the π^- mesons were obtained from a study of the elastic events. Wire tests of the magnet system and calculation of trajectories through the collimation system also support these values. The μ^- and e^- contamination in the beam was 16.8±0.5%: 16.1% μ^- and 0.7% e^-.[13]

There were 1841 $\pi^-\pi^+n$, 1316 $\pi^-\pi^0p$ and 4728 elastic events found in 33 000 pictures. The number of beam tracks per picture varied widely, averaging about 15 tracks per picture. The pictures and chamber conditions were sufficiently uniform that ionization could usually be used to separate π^+ from protons.

The film was scanned twice, two views at a time for zero-, one-, two-, three-, or four-prong events. The beam tracks were viewed along their path to increase scanning efficiency for elastic events with short-range protons. A high scanning efficiency was also achieved for the single-pion-production events since the maximum possible secondary π^- kinetic energy is 460 MeV, corresponding to a 20% reduction in radius of curvature. Each event was sketched on a scanning sheet with bubble density estimates for each track. Double scatterings and associated electron pairs were drawn when observed. From the two scans, the scanning efficiency for two-prong events was estimated to be greater than 99% except for systematic corrections for small-angle elastic scattering and events for which the plane of the charged secondary particles was parallel to the optic axis of the camera system.

The two-prong events were measured with an Itek Precision Film Reader with punched card output, and were analyzed with spatial reconstruction and

[9] G. B. Yodh, T. B. Day, G. Quareni, A. Quareni-Vignerdelli, R. A. Burnstein *et al.*, Bull. Am. Phys. Soc. 8, 68 (1963), and to be published.

[10] E. Ferrari and F. Selleri, Phys. Rev. Letters 7, 387 (1961); Nuovo Cimento Suppl. 24, 453 (1962).

[11] E. L. Hart, Brookhaven National Laboratory, 1962 (unpublished).

[12] J. Martin (private communication).

[13] Measurements of the beam composition were made by the Carnegie Tech group with counters including a CO_2 Čerenkov counter.

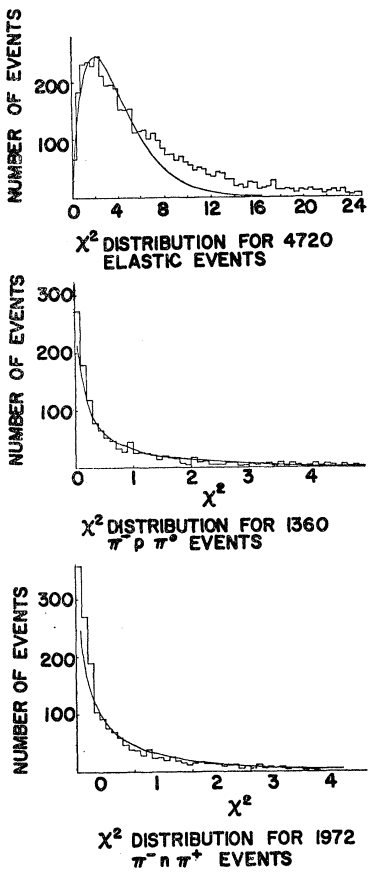

FIG. 2. The χ^2 distributions for the elastic and inelastic reactions, with the theoretical distributions shown by solid curves.

GUTS kinematic analysis programs for the IBM-709 computer.[14]

An analysis of the adjustments made by the fitting program to the measured momenta for an initial group of elastic events led to a refinement of the values assumed for the beam momentum and the magnetic field, to the inclusion of a correction for energy loss along the path of the particle, and to the calculation of momentum from range for stopping particles. The final distributions of DK, the fractional adjustment of the measured curvatures, shown in Fig. 1, are satisfactorily symmetric.

The GUTS analyses were made for the following classifications:

$$\pi^- + p \rightarrow \pi^- + p, \qquad (-p)$$
$$\pi^- + p \rightarrow \pi^- + p + \pi^0 \qquad (-0p)$$
$$\pi^- + p \rightarrow \pi^- + n + \pi^+ \qquad (+-n).$$

The program calculated the χ^2 goodness-of-fit parameter, the expected bubble density as seen on the scanning table, and a measure of the coplanarity of the event, for each interpretation.

[14] J. P. Berge, F. T. Solmitz, and H. D. Taft, Rev. Sci. Instr. 32, 538 (1961).

To ensure that the events were produced by beam tracks of the correct momentum, the following criteria were imposed: The measured beam momentum had to be between 575 and 887 MeV/c when the measured track length was greater than 10 cm; the measured beam direction had to be within 5° of the average beam direction.

The χ^2 limits chosen were 6.64 for inelastic events and 13.28 for elastic events. These values correspond to a 1% probability of a greater χ^2 for that event type. The angle between the beam track and the plane of the two outgoing tracks was required to be less than 10° for elastic events. Each event was examined along with the computer output for the event so that classification could be made. Of the events associated with beam tracks and within a circular scanning region, 57% were classified on the first measurement and eventually 94% of the measured events were classified in one of the three categories. The remainder could not be classified because of: a short track due to a secondary scattering or decay, a very steep track, a picture with poor illumination or badly regulated ionization, or, finally, multiple pion production. Figures 2 and 3 show the χ^2 and the missing mass distributions for the events thus selected.

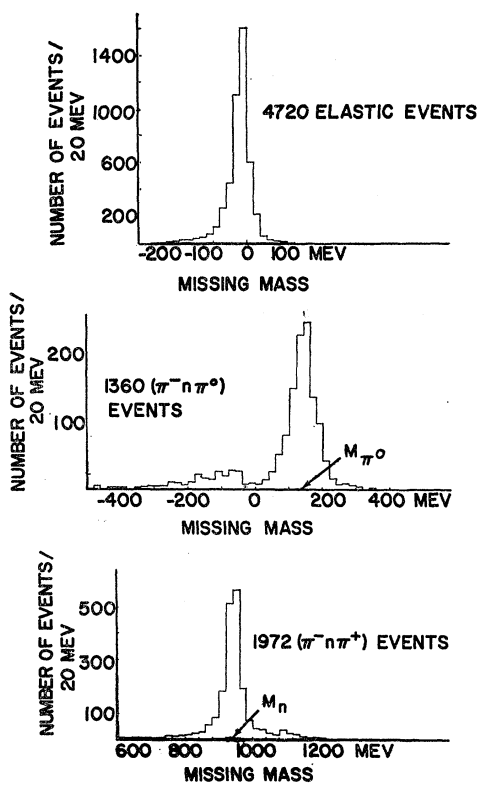

FIG. 3. The missing mass distributions for the elastic and inelastic reactions.

TABLE I. Summary of the quantities used in the cross-section calculations.

Reaction	No. in scan circle	No. in fid. region	Correction factors	Cross sections (mb)
$\pi^- p$	721	401	1.0360±0.0028[a] 1.023 ±0.011[b]	18.9 ±1.3
$\pi^- p\pi^0$	189	105	1.071 ±0.017[b]	4.98±0.54
$\pi^- n\pi^+$	275	152	1.167 ±0.034[b]	7.87±0.91
All-neutral	569	316		14.0 ±1.0
Mult. π prod.	7	4		<0.2 mb
All meas. 2-prong events	1081	603		σ_T=45.9 ±1.9

[a] Correction for bias against short-range protons.
[b] Corrections for azimuthal scanning bias.

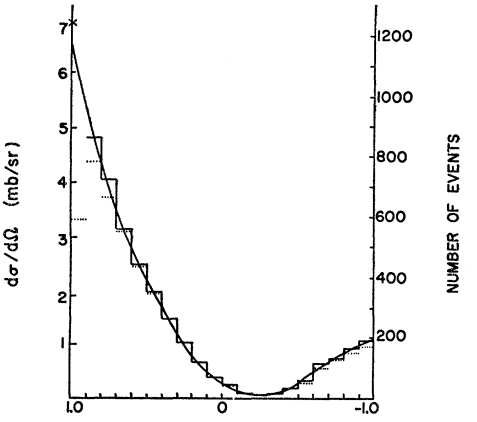

FIG. 5. Differential cross section for elastic scattering, with the forward scattering point obtained from dispersion theory and the optical model shown by the cross at 0°. Values uncorrected for scanning bias are shown by dotted lines.

III. CROSS SECTIONS

The best nine rolls of film, containing 5800 pictures, where chosen for the cross-section determination. In these rolls there was an average of 11 beam tracks per picture, although some pictures had up to 34 beam tracks. To be accepted a beam track had to enter the thin window of the bubble chamber at an angle within ±5° of the average projected entrance angle for tracks of correct curvature, and to have the correct projected curvature (within 5%) as measured on the scanning table with a template curve of radius 90 in. These nine rolls were scanned twice and the beam tracks counted in every picture.

A restricted fiducial region for the cross-section calculation was formed by requiring the interaction point to have coordinates within a volume 12×10×10 cm. About 50% of the events were in this region. The average length of a beam track crossing this region was found to be 12.173 cm after corrections for curvature, skew, and dip.

After corrections for beam contamination, for loss in path length due to interactions, and for nonbeam tracks, the number of acceptable pion tracks was 49 413±561. The density of the liquid hydrogen was determined from a neon vapor-pressure thermometer in contact with the bubble chamber and from empirical temperature-density relations. While the pictures were being taken the neon vapor pressure was 51±1 cm of mercury. The experimental curves give a corresponding density of 0.0626±0.0001 g/cc.[11] The error was estimated from the curves, using a ±1-cm-Hg variation of the vapor pressure. These values were used in all cross-section calculations.

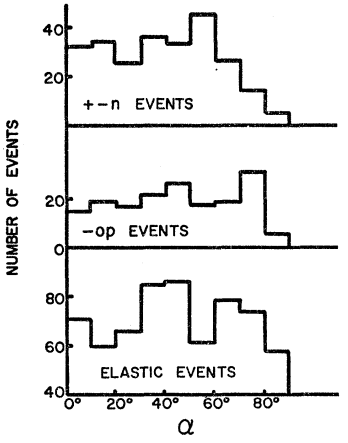

FIG. 4. Distribution of α, the angle between the front glass plane and the plane of the outgoing charged particles.

In three scans of the two-prong events (approximately 100% efficient) 640 elastic events, 168 π^0 production events, 244 π^+ production events, and 7 multiple-pion-production events were found in the scanning region. In addition, there were 5 events which were ambiguous and 128 events which for one reason or another were unmeasurable, which were distributed in ratios determined from the identified events. In the scanning region, 478 zero-prong events were found in one scan with an efficiency of 84%, calculated from other scans of the zero-prong events. The results are summarized in Table I, after corrections for scanning efficiency and for the 133 unclassified two-prong events.

A scanning bias exists against events for which the plane of the two secondary prongs is parallel to the camera axis. Correction factors were obtained by plotting the number of events found in intervals of α, the angle between the plane of the two prongs and the front glass plane of the bubble chamber; the results are shown in Fig. 4. A bias is expected against events with α near 90°; the corresponding corrections are given in Table I. These factors were calculated from consideration of the variation of azimuthal angle distribution with the c.m. scattering angle; the corrected and uncorrected scattering-angle distributions are compared in Fig. 6. Fitting the corrected data to a simplified optical model to account for the loss of elastic events with very short range protons contributed an additional correction factor of 1.0360±0.0028.

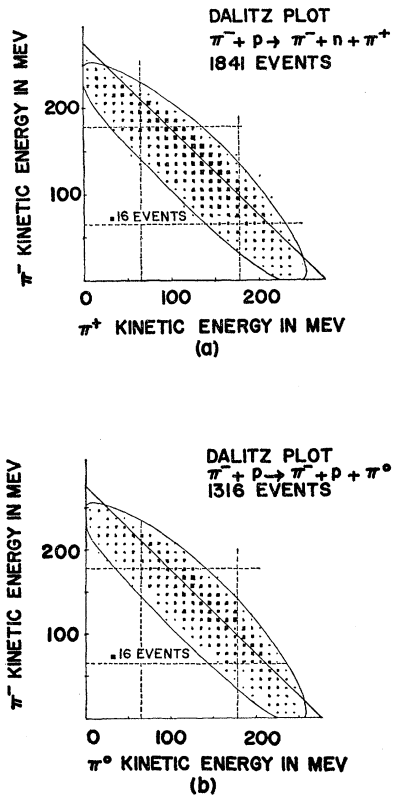

FIG. 6. Dalitz plots for the $\pi^- n\pi^+$ and $\pi^- p\pi^0$ reactions. The solid outline represents the kinematic limits for pion production with incident momentum 731±20 MeV/c. The dashed lines correspond to pion recoil from an isobar of mass 1223±70 MeV.

IV. ELASTIC SCATTERING

The c.m. angular distribution for the 4728 elastic events, Fig. 5, was fitted to the following polynomial by the least-squares method:

$$\frac{d\sigma(\text{mb})}{d\Omega(\text{sr})} = (0.300\pm0.020)+(1.94\pm0.15)\cos\theta + (3.82\pm0.27)\cos^2\theta-(0.41\pm0.10)\cos^3\theta - (0.35\pm0.16)\cos^4\theta+(1.19\pm0.24)\cos^5\theta.$$

The coefficients are normalized to the elastic cross section given in Table I. Due to the scanning bias against elastic events with small scattering angles, the events with $\cos\theta>0.9$ were not used with the fit. As a check, the fitting was repeated with a cutoff at $\cos\theta=0.8$, with no essential change in the coefficients, and with a fifth-order polynomial still giving the best fit to the data. A more detailed discussion of the elastic scattering is given elsewhere.[15]

The forward-scattering point in Fig. 6, calculated from dispersion theory and the optical model,[16] is consistent with the fifth-order polynomial. The need for fifth-order terms suggests that F-wave interference is already important in the vicinity of the total cross-section peak, although the D-wave scattering amplitude still dominates. Grard *et al.*[17] have reported similar results at a slightly higher energy.

V. SINGLE PION PRODUCTION

The significant kinematic features of both pion-production channels are evident in the Dalitz plots of Fig. 6. A uniform density of events within the kinematic bounds is to be expected from simple phase-space dependence, while excitation of the $N^*(3,3)$ isobar of mass 1223 MeV should be reflected in concentrations about the recoil pion axes, within the half-width limits shown by the dotted lines. Neither effect seems to be especially pronounced; instead, the predominant effect seems to be a concentration of events about a diagonal which intersects the pion kinetic-energy axes at 275 MeV.

This is seen more clearly in the two-pion effective-mass distributions, Fig. 7, where a broad peaking appears in the vicinity of 520 MeV. This rise is clearly inconsistent with straightforward phase-space dependence, or with the isobar model of Lindenbaum-Sternheimer, and is pronounced in both pion-production

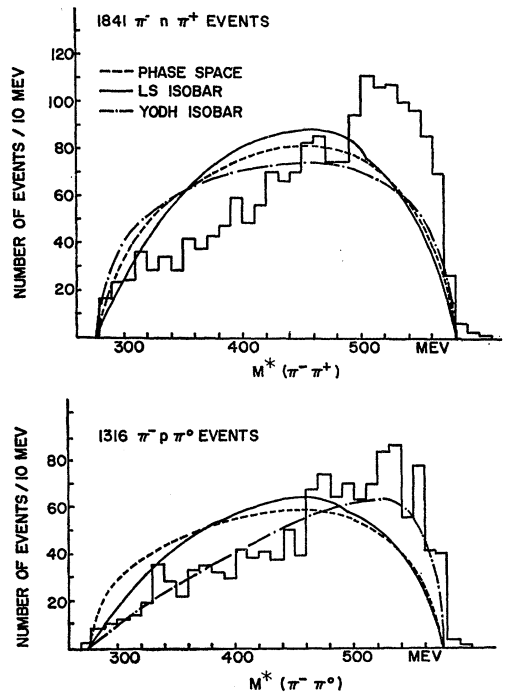

FIG. 7. Two-pion effective mass distributions for the $\pi^-\pi^+$ and $\pi^-\pi^0$ systems. Predictions of phase-space dependence, the LS isobar model, and the Olsson-Yodh isobar model are shown for comparison.

[15] B. R. Riley, M.S. thesis, University of Kentucky, 1963 (unpublished).
[16] J. W. Cronin, Phys. Rev. **118**, 824 (1960).
[17] F. Grard, G. McLeod, L. Montanet, M. Cresti, R. Barloutaud *et al.*, Nuovo Cimento **22**, 193 (1961).

channels. Peaking in the $\pi^-\pi^+n$ reaction has previously been noted by Kirz and co-workers[18] at incident pion energies of 360–780 MeV; the fact that the location of the peak in the effective mass distribution is different at each incident energy, lying always just below the kinematic maximum, precludes interpretation in terms of a dipion state with fixed excitation energy.

Momentum distributions for the pions, Figs. 8 and 9, and nucleons, Fig. 10, are compared with the predictions of phase space and the Lindenbaum-Sternheimer (LS) isobar model. The relative mixing of the $J_{\pi,1}$ and $J_{\pi,2}$ decay and recoil momentum spectra in the latter are determined by branching parameters ρ and a, in the LS notation, which yield ϕ, the phase difference between matrix elements for producing the isobar in the I-spin $\frac{1}{2}$ and $\frac{3}{2}$ states. From counter values[19] of $\sigma(I=\frac{1}{2})=21$ mb and $\sigma(I=\frac{3}{2})=3$ mb, and the ratio $R=\sigma(\pi^-\pi^0 p)/\sigma(\pi^-\pi^+ n)=0.633$ obtained in the present experiment, the values $\rho=0.072$, $a=-0.123$, and $\phi=120.7°$ were determined for the momentum distributions shown. There seems to be considerable evidence of isobar formation, although deviations from the detailed

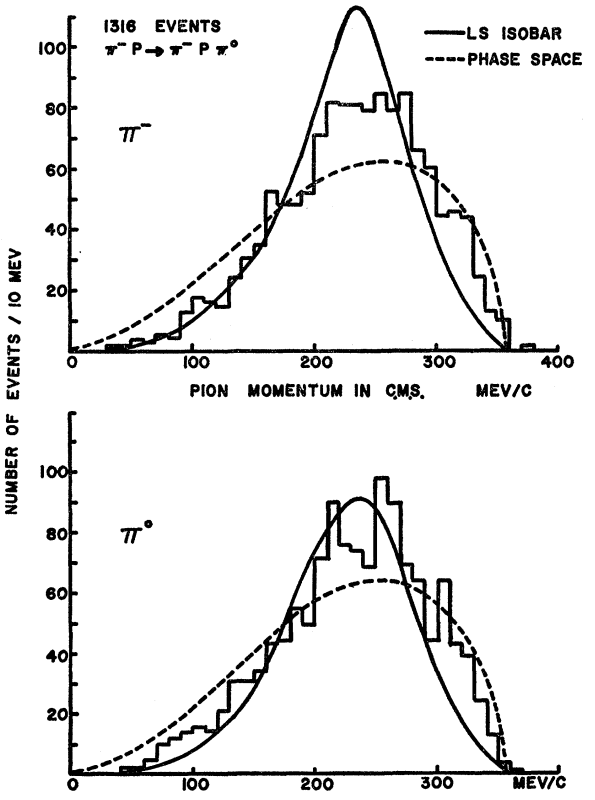

FIG. 8. Momentum distributions for the π^- from the $\pi^-n\pi^+$ and $\pi^-p\pi^0$ reactions. Predictions of phase-space dependence and the LS isobar model are shown in comparison.

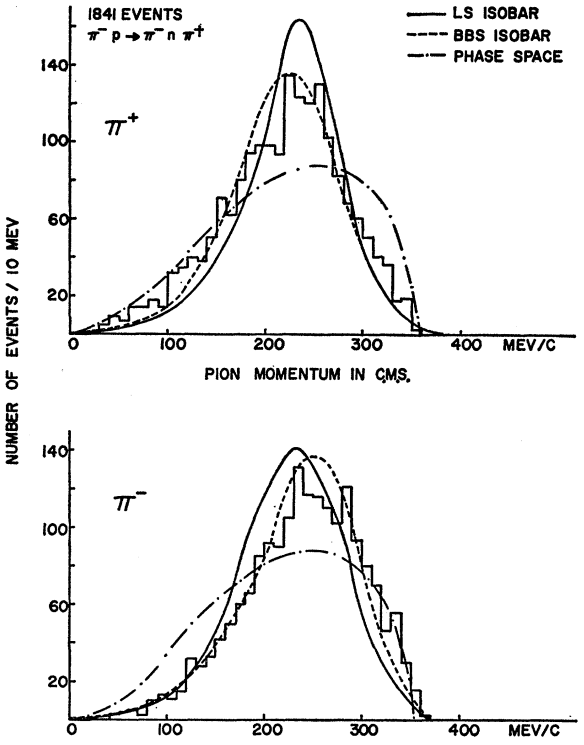

FIG. 9. Momentum distributions for the π^+ from the $\pi^-n\pi^+$ reaction and the π^0 from the $\pi^-p\pi^0$ reaction. Predictions of phase-space dependence and the isobar models are shown for comparison.

LS model predictions are very evident, most notably in the nucleon distributions.

The center-of-mass (c.m.) scattering angles for the $\pi^-\pi^0 p$ reaction, Fig. 11, show complete isotropy, while there is some suggestion of forward and backward peaking for the pions in the $\pi^-\pi^+n$ production state, Fig. 12. For the most probable isobar pairing, the π^-n in this latter reaction, the angle distribution for the π^- in the π^-,n rest frame has been calculated. A decided forward-backward asymmetry, similar to that observed recently at much higher incident energy, 4 BeV/c,[20] is evident for events both inside and outside the isobar mass half-width. This further demonstrates that mechanisms other than simple isobar production are important in this channel.

The Lindenbaum-Sternheimer formalism assumes complete isotropy in the production and decay of the isobar in the overall center of mass system. Bergia, Bonsignori, and Stanghellini[21] (BBS) have, however, pointed out that incoherent summing of the contributions from the separate pion-nucleon formation possibilities is not justified except in the limit of a stable isobar, and have demonstrated the necessity for including isobar interference terms. Inclusion of the BBS

[18] J. Kirz, J. Schwartz, and R. D. Tripp, Phys. Rev. **130**, 2481 (1963).

[19] P. Falk-Vairant and G. Valladas, Rev. Mod. Phys. **33**, 362 (1961).

[20] Aachen-Birmingham-Bonn-Hamburg-London (I. C.)-München Collaboration, Nuovo Cimento (to be published).

[21] S. Bergia, F. Bonsignori, and A. Stanghellini, Nuovo Cimento **16**, 1073 (1960).

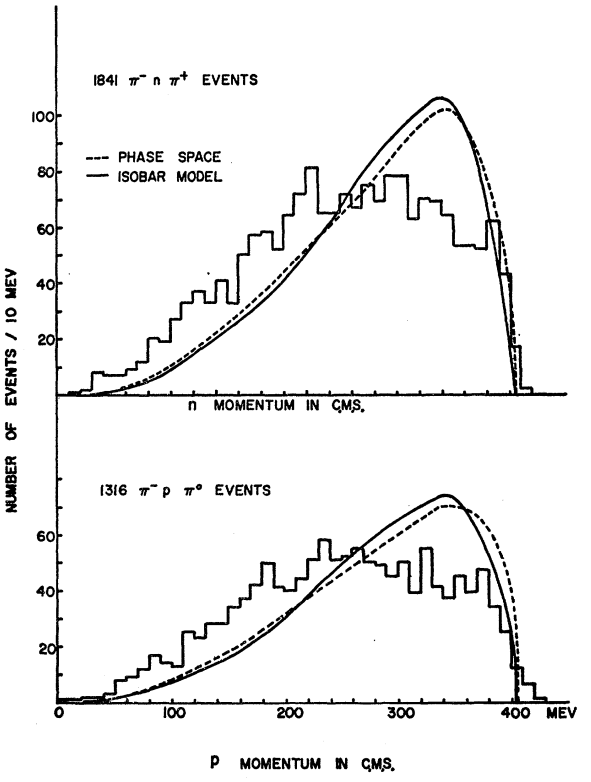

FIG. 10. Momentum distributions for the nucleons from the $\pi^-n\pi^+$ and $\pi^-p\pi^0$ reactions. Predictions of phase-space dependence and the LS isobar model are shown for comparison.

interference appears to improve the momentum distribution fit, Fig. 9. In the case of π^+p scattering at the same energy, however, the Saclay group[22] has shown that the pion momenta demonstrate none of the double peaking expected for BBS interference in the pure $I=\frac{3}{2}$ production state.

A further modification of the isobar model to include the possibility that the isobar is formed with the Z component of its spin aligned along the incoming beam direction and decays with a $1+3\cos^2\theta$ distribution with respect to the isobar direction has been proposed by Olsson and Yodh.[23] They assume S-wave production, as is indicated by angular distributions measured at 550–600 MeV and at lower energies, and include the requirements of Bose statistics. Inclusion of the P-wave decay term effectively smooths out the sharp peaking in the $T=\frac{3}{2}$ momentum and energy distributions predicted by the BBS isobar model.

The Yodh model appears to account for many of the characteristic kinematic features of the π^+,p interaction, particularly the $\pi-\pi$ Q values, at energies from 558 to 1090 MeV. This model provides an excellent fit to the $\pi^-\pi^0$ effective-mass distribution in the present experiment, Fig. 7, but fails to predict the observed $\pi^+\pi^-$ mass distribution, Fig. 7.

The peaking effect in effective-mass distributions seems equally prominent for $\pi^-\pi^0$ and $\pi^+\pi^-$ systems. If the same mechanism is responsible for the peaking in both cases, this would present considerable difficulty for the Yodh isobar model, which requires coherent interference which would be constructive for $\pi^-\pi^0$ production and destructive for $\pi^+\pi^-$.

Yodh has suggested the possibility that the mass effects observed are of different origin, the $\pi^+\pi^-$ "peaking" appearing as a consequence of destructive interference with a strong $I=0$ $\pi\pi$ scattering, which acts to deplete the region near the lower phase-space boundary. The $I=0$ $\pi\pi$ scattering length is expected to be appreciable from a variety of considerations. The ABC experiment[7] and theoretical arguments[24] suggest that the $I=0$ $\pi\pi$ interaction may be resonant, although the $\pi^+\pi^-$ mass distribution, Fig. 7, gives no evidence of peaking near the dipion threshold, at the resonance energy expected.

The possibility remains that such $\pi\pi$ peaking tends to be washed out through interference with the isobar production channel. The question of whether interference effects have depleted the density of events with low $\pi\pi$ mass in the region of high isobar production probability has been explored by dividing the Dalitz plot for the $n\pi^+\pi^-$ reaction into the nine regions shown

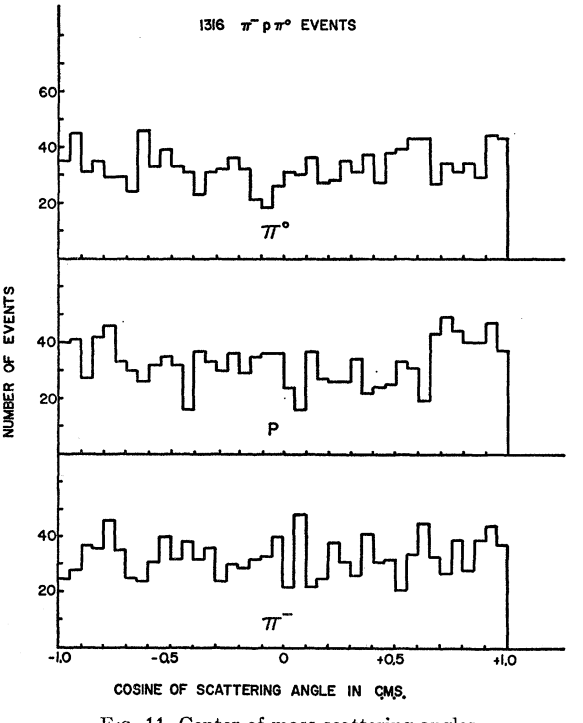

FIG. 11. Center-of-mass scattering angles for the $\pi^-p\pi^0$ reaction.

[22] R. Barloutaud, L. Cardin, A. Derem, G. Gensollen, A. Leveque *et al.*, Nuovo Cimento **26**, 1409 (1963).
[23] M. Olsson and G. Yodh, Phys. Rev. Letters **10**, 353 (1963).
[24] N. Wu and G. Z. Yang, Sci. Sinica (Peking) **12**, 317 (1963).

TABLE II. Number of events per 100 MeV² in the 9 Dalitz plot sections of Fig. 13.

Section	Number of events/100 MeV²
a	15.3±2.5
b	33.1±1.4
c	27.8±3.3
d	11.6±1.6
e	24.1±1.5
f	18.5±2.1
g	6.9±1.4
h	20.6±1.2
i	15.8±2.1

in Fig. 13. The density of events per hundred MeV² in each of the nine regions is listed in Table II; the estimated error takes into account area measurement as well as number of events. The relative densities of low-dipion-mass events in the energy region of highest isobar probability, where the greatest interference is expected, $h/(e+b)=0.36\pm0.07$, showing no depletion compared to similar ratios for smaller isobar-production probability, $g/(d+a)=0.26\pm0.06$ and $i/(f+c)=0.34\pm0.05$. In the perpendicular direction, the ratio of densities outside and inside the energy region of highest isobar-production probability is, if anything, smaller at low-dipion-mass values than at high, with

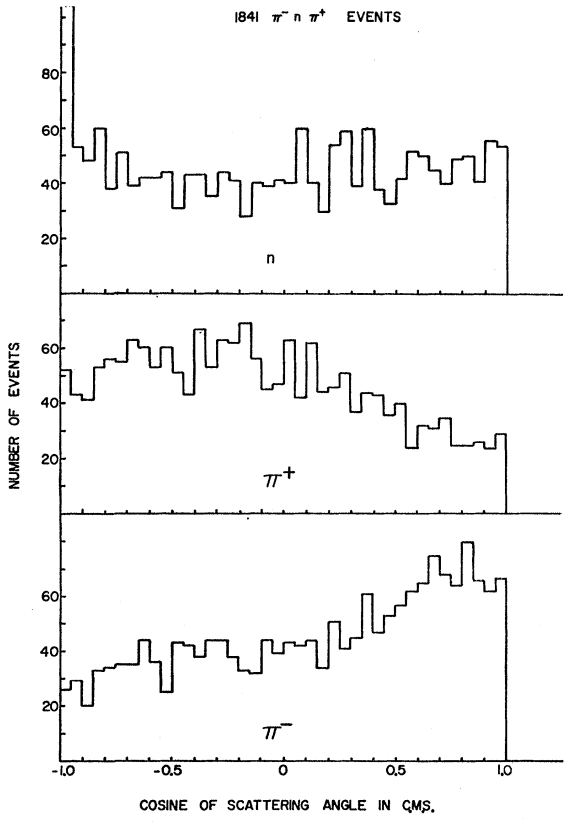

FIG. 12. Center-of-mass scattering angles for the $\pi^-n\pi^+$ reaction.

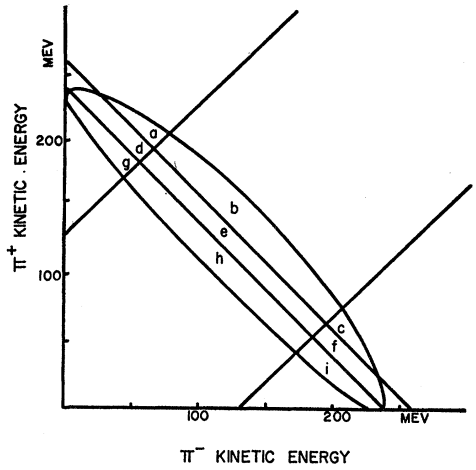

FIG. 13. Division of the Dalitz plot for the $\pi^-n\pi^+$ reaction into sections for interference study. Diagonals from upper left to lower right divide 3 regions of equal dipion production area, while the intersecting diagonals mark off regions inside and outside the approximate isobar-production half-width.

$(g+i)/h=0.55\pm0.09$, compared to $(d+f)/e=0.63\pm0.09$ and $(a+c)/b=0.66\pm0.09$. In either case, no depletion effects in region h, where interference effects are expected to be strongest, are observed.

As shown in Fig. 14, a rather good fit to both $\pi^+\pi^-$ and $\pi^-\pi^0$ effective-mass distributions is obtained by integrating the Chew-Low equation,[25]

$$\frac{d^2\sigma}{d\omega^2 d\Delta^2}=\frac{f^2}{2\pi}\frac{\Delta^2/\mu^2}{(\Delta^2+\mu^2)^2}\frac{\omega(\frac{1}{4}\omega^2-\mu^2)^2}{q_{in}^2}\sigma_{\pi\pi}(\omega),$$

over Δ^2, the four-momentum transfer term, assuming $\sigma_{\pi\pi}$ to be constant or slowly varying at energies well below the ρ threshold. However, integrating over the square of the dipion effective mass, ω^2, under the same assumption fails to give agreement with the nucleon kinetic energy spectrum, Fig. 15. The nonperipheral nature of the scattering interaction is further suggested by the isotropy of the nucleon angle distributions[26] in Figs. 11 and 12. No reasonable choice of energy or

[25] G. F. Chew and F. E. Low, Phys. Rev. **113**, 1640 (1959).

[26] The prominent peaking of neutrons in the extreme backward c.m.s. direction for the $\pi^-n\pi^+$ events, Fig. 12, merits comment. Such an effect might be expected from spurious fits of elastic events to inelastic scattering categories using incorrect values of the beam momentum, the nonexistent "neutrals" appearing to be produced parallel to the beam direction. This effect should show up most strongly, however, in the $\pi^-p\pi^0$ events whose neutral-particle angle distribution, Fig. 11, is uniformly isotropic. All of the π^+ lab momenta for the selected neutron-backward events were below 600 MeV/c, so that ionization information was reliable in identifying the positive particles. The χ^2 distributions for the selected events and for the total sample were in good agreement, as were the neutron c.m.s. momentum distributions. It appears likely that the backward neutron peaking in the smallest interval of c.m.s. angle is a real effect, indicating that some peripheral pion-pion interaction occurs in the $T=0$ state, probably in the S wave. The neutron energy distribution in the lab system is strongly peaked at zero for these events, with no neutrons above 80 MeV in kinetic energy. The events with this strong directional collimation amount to some 3% of the total of the $\pi^-n\pi^+$.

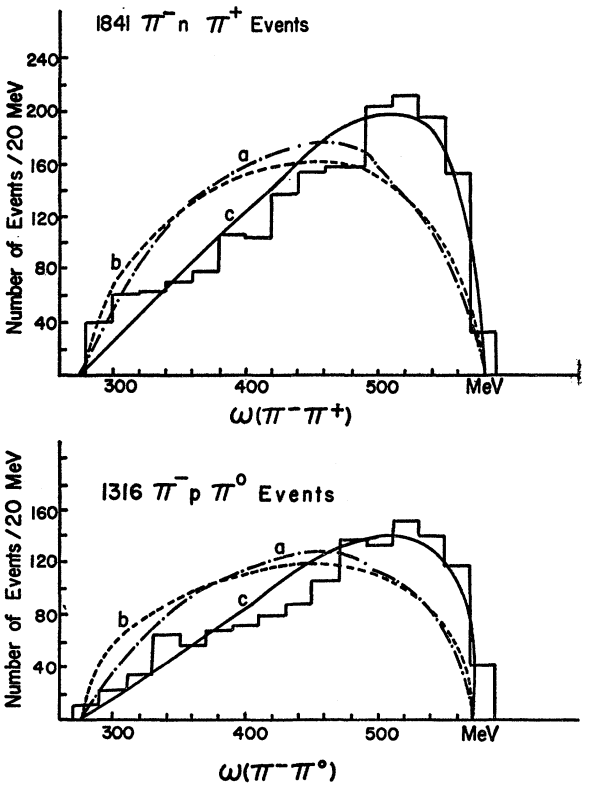

FIG. 14. Distributions of effective mass of the pion-pion system compared with calculations from the LS isobar (a), phase-space dependence (b), and from the Chew-Low equation assuming $\sigma_{\pi\pi}$ constant, (c).

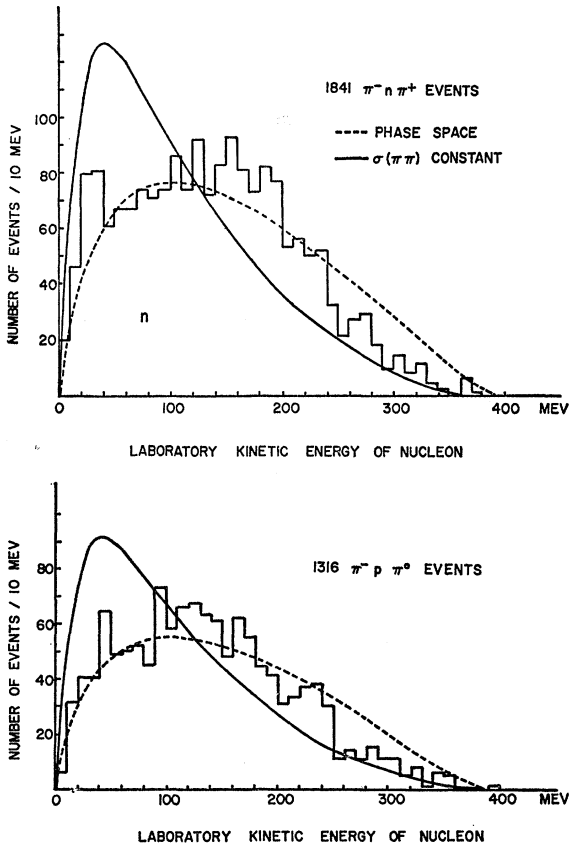

FIG. 15. Distributions of the nucleon laboratory kinetic energy compared with calculations from phase space (dashed curve), and from the Chew-Low equation assuming $\sigma_{\pi\pi}$ constant.

momentum dependence for $\sigma_{\pi\pi}$ provides a satisfactory fit to both distributions, Figs. 14 and 15; the $\Delta^2/(\Delta^2+\mu^2)^2$ term in the Chew-Low equation continues to dominate the nucleon kinetic-energy spectrum. Including the $I=0$ S-wave cross section calculated by Wu and Yang[24] (the $I=2$ S-wave $\pi\pi$ scattering is negligibly small at these energies) only has the effect of further enhancing the predicted low-energy peaking of the nucleon energy distribution, near 40 MeV.

There seems to be no very simple explanation of the peaking in the $\pi\pi$ effective-mass distributions. Singularities associated with "triangular" Feynman diagrams have been shown capable[27] of leaving the outgoing pions in a state of high relative energy, but the peaking falls off much more rapidly with energy than is the case with the present effect, which is still very prominent at 558 MeV.[9] Selleri[28] has pointed out that higher order rescattering diagrams, or exchange terms in suitable combination, might lead to effects such as those here observed; presumably the complete explanation will involve a considerable admixture of isobar production as well.

[27] P. V. Landshoff and S. B. Trieman, Phys. Rev. **127**, 649 (1962); R. Aaron, Phys. Rev. Letters **10**, 32 (1963).
[28] F. Selleri (private communication).

ACKNOWLEDGMENTS

The authors wish to thank the Cosmotron staff and L. Leipuner and R. K. Adair for their assistance with beam and bubble chamber in this experiment. The aid of A. Erwin, J. Boyd, and L. Leipuner in programming, of J. Forehand of the Texas A & M Data Processing Center, and of the Computing Center of the University of Kentucky are gratefully acknowledged. Particular thanks are due to G. Yodh for isobar-model calculations and for very helpful discussion, and to our loyal scanning and measuring staff who were indispensible to this experiment.